Energy dependence, kinetic isotope effects, and thermochemistry of the nearly thermoneutral reactions $N^+(^3P)+H_2(HD,D_2)\rightarrow NH^+(ND^+)+H(D)$

Kent M. Ervin and P. B. Armentrout[a)]
Department of Chemistry, University of California, Berkeley, California 94720

(Received 15 October 1986; accepted 28 November 1986)

The reactions of $N^+(^3P)$ ions with H_2, HD, D_2 are examined using guided ion beam tandem mass spectroscopy. Absolute reaction cross sections are measured from near thermal energies to 30 eV relative energy. The low energy cross section behavior is analyzed using empirical threshold models and phase space theory. The results are compared to other recent studies of the $N^+ + H_2$ system. The reaction endothermicity for $N^+(^3P) + H_2 \rightarrow NH^+ + H$, $\Delta H^\circ_0 = 0.033 \pm 0.024$ eV (0.76 ± 0.55 kcal/mol), and the bond energy of NH^+, $D^\circ_0(N\text{–}H^+) = 3.51 \pm 0.03$ eV (80.9 ± 0.6 kcal/mol), are derived from the results.

INTRODUCTION

The hydrogen atom transfer reaction

$$N^+(^3P) + H_2 \rightarrow NH^+ + H \qquad (1)$$

has served as a model system in the study of the kinetics and dynamics of ion–molecule reactions. Reaction (1) is interesting from a dynamics standpoint because it is nearly thermoneutral and the NH_2^+ intermediate is a known stable species. Differential reactive scattering measurements[1–6] of reaction (1) and its isotopic variants

$$N^+(^3P) + D_2 \rightarrow ND^+ + D, \qquad (2)$$

$$N^+(^3P) + HD \rightarrow NH^+ + D \qquad (3a)$$

$$\rightarrow ND^+ + H \qquad (3b)$$

has shown that at low collision energies the reactant mechanism involves a long-lived intermediate complex. At higher energies, the reaction mechanism becomes direct. The reaction dynamics were originally interpreted by Mahan and coworkers[1–5] using predictions of the NH_2^+ potential energy surfaces obtained by construction of electronic state correlation diagrams.[7] *Ab initio* potential energy surface calculations,[8–13] particularly in regions of critical surface crossings identified by the correlation diagrams, complement the experimental dynamics studies. The theoretical potential energy surfaces indicate that access to the NH_2^+ well is permitted at low reaction energies, thus promoting a long-lived complex mechanism.[10,13] Nonadiabatic transitions between low-lying electronic surfaces may be responsible for the direct reaction mechanism at higher energies.[11,12]

Interest in reaction (1) has been rekindled recently by its role as a possible first step in the synthesis of ammonia in interstellar clouds.[14] Knowledge of the temperature dependence and kinetic energy dependence of the reaction is important for modeling the chemistry of nitrogen-containing species under the conditions of interstellar space.[15] Since reaction (1) is nearly thermoneutral, the expected temperature dependence of the rate depends critically on the magnitude and direction of the reaction enthalpy. However, the reaction energetics are not known precisely due to experimental uncertainties in the heat of formation of NH^+.

Experimental reaction rates for reaction (1) at 300 K are tabulated in Table I. The most recent experiments indicate that the rate at 300 K is 20%–30% of the collision rate predicted by the Langevin–Gioumousis–Stevenson (LGS) model for ion–induced dipole interactions.[16] Recent experiments at very low temperatures have established that the reaction rate decreases rapidly with decreasing temperature. The reaction has been studied from 8 to 70 K in a supersonic gas jet[17] and from 11 to 20 K in a low temperature ion trap.[18] Arrhenius analysis of these data combined with the 300 K reaction rate (Table I) indicate that reaction (1) has an activation energy of either 4 meV[17] or 7.4 ± 0.8 meV.[18]

The rates for reactions (1), (2), and (3) have also been measured as a function of relative kinetic energy by the selected-ion flow/drift tube (SIFDT) technique.[19] An analysis of the kinetic energy dependence of the reaction rate

TABLE I. $N^+ + H_2 \rightarrow NH^+ + H$ reaction rates at 300 K.

Technique[a]	$k(10^{-10}$ cm^3 s$^{-1})$
FA[b,c]	4.7
ICR[c]	4.8
SIFT[d]	6.4
SIFT[e]	4.8
SIFT[f]	6.2
SIFDT[g]	3.7
GB[h]	3.9 ± 0.8
LGS[i]	15.8

[a] FA, flowing afterglow; ICR, ion cyclotron resonance; SIF(D)T, selected-ion flow (drift) tube; GB; guided beam; LGS, Langevin–Gioumousis–Stevenson collision rate model.
[b] F. C. Fehsenfeld, A. L. Schmeltekopf, and E. E. Ferguson, J. Chem. Phys. **46**, 2802 (1967).
[c] J. K. Kim, L. P. Theard, and W. T. Huntress, Jr., J. Chem. Phys. **62**, 45 (1975).
[d] N. G. Adams and D. Smith, Int. J. Mass Spectrom. Ion Phys. **21**, 349 (1976).
[e] D. Smith, N. G. Adams, and T. M. Miller, J. Chem. Phys. **69**, 308 (1978).
[f] M. Tichy, A. B. Rakshit, D. G. Lister, and N. D. Twiddy, Int. J. Mass Spectrom. Ion Phys. **29**, 231 (1979).
[g] Reference 19.
[h] This work.
[i] Reference 16.

[a)] Presidential Young Investigator, 1984–1988; Alfred P. Sloan Fellow, 1986–1988.

yields an endoergicity (at 300 K) of 11 ± 3 meV for reaction (1) and 33 ± 4 meV for reaction (2).[19] The deviation between reactions (1) and (2) is attributable to the different zero-point vibrational energies of H_2, D_2, NH^+, and ND^+. Similarly, the two channels of reaction (3) have different energetics due to zero-point energy differences such that reaction (3a) is endothermic by 43 ± 6 meV and reaction (3b) is slightly exothermic according to the SIFDT results.[19] This variation of the energetics of reactions (1), (2), (3a), and (3b) establishes unambiguously that the observed activation energies are due to the thermochemical endoergicities, rather than a potential energy barrier.

The energy spacings of the H_2 rotational levels ($B_e = 121.3\ cm^{-1} = 15$ meV) are of the same order of magnitude as the experimental activation energy. Therefore, it is important to take into account the rotational energy when comparing the activation energies obtained by different experiments. The authors of the low temperature experiments corrected the activation energies to 0 K by simply subtracting the mean available rotational energy under the experimental conditions (taking into account the experimental populations of *ortho* and *para* hydrogen). This implicitly assumes that rotational and kinetic energy are equivalent in driving the reaction. The corrected activation energies obtained are 22 meV for the gas jet experiment[17] and 18.5 meV for the ion trap experiment.[18] Making the same rotational energy correction for the endothermicity derived from the 300 K SIFDT results gives a 0 K endothermicity of 37 ± 3 meV for reaction (1). While the deviations between the various experiments are not large in absolute terms for thermochemical measurements of this type, confidence in the endothermicity value would be bolstered by better relative agreement. The role of rotational energy in promoting the reactions needs further consideration.

Surprisingly, there have been no published measurements of the absolute integral cross sections for reactions (1), (2), and (3), although Eisele *et al.* have reported relative cross sections for reaction (1) from 0.9 to 5.5 eV based on measurements on a differential scattering apparatus.[6] In the present work, guided ion beam techniques are used to examine the kinetic energy dependence of the integral reaction cross sections. The guided beam technique spans the energy range from near thermal to tens of electron volts in relative energy. The cross sections at low energies are analyzed to obtain the heats of reaction for comparison with the results of the thermal[19] and subthermal[17,18] rate measurements. We discuss how the extracted thermochemical values are affected by spin-orbit splittings, excited product states, and the assumptions used to analyze the experiments. The effect of H_2 rotational energy on the reaction cross sections is considered both empirically and within the framework of phase space theory. The cross section behavior and isotope effects are compared to the dynamic information obtained by the differential cross section measurements of Mahan and co-workers.[1-5]

EXPERIMENTAL METHODS

The guided ion beam apparatus and data reduction procedures are described elsewhere.[20-22] A brief outline of the experimental technique is included here along with details pertinent to reactions (1), (2), and (3).

Guided ion beam apparatus

The guided ion beam apparatus is similar to conventional ion beam/gas cell instruments used to measure total reaction cross sections. Ions are extracted from the ion source (described below), focused into a beam, and mass analyzed in a magnetic sector to select the desired species. The ions are then refocused and injected at the desired ion kinetic energy into a radio-frequency octopole ion beam guide. The octopole is the heart of the apparatus. It creates a radial potential well along the axis of the ion beam which traps ions in radial directions but does not affect their axial velocities. The octopole acts as an ion "pipe" which passes through the gas collision cell and collects scattered product ions with near 100% efficiency. This trapping greatly improves the sensitivity compared to conventional beam/gas cell instruments and avoids artifacts due to different collection efficiencies for product ions scattered in different directions. The octopole also allows operation of the ion beam at low energies (down to 0.1 eV lab), where the beam would become dispersed without the trapping field due to space charge effects and focusing aberrations. Product ions and unreacted primary ions drift to the end of the octopole, are extracted from it, mass analyzed with a quadrupole mass filter, and detected by secondary electron scintillation and pulse counting electronics.

Reaction cross sections are obtained from the reactant and product ion intensities, the gas cell pressure, and the estimated reaction path length.[20] The relative uncertainty of the cross sections at different energies and for different reactions is within 5% for cross sections greater than $10^{-17}\ cm^2$ and is limited by statistical counting uncertainties for smaller cross sections. The uncertainty in the absolute magnitude of the cross sections is limited mainly by the gas pressure measurement and by the estimate of the reaction path length. We estimate that the error in the absolute cross sections from all sources is $\pm 20\%$.[20]

The absolute kinetic energy of the ion beam is measured by utilizing the octopole itself as a retarding energy analyzer. Since the interaction region and the energy analysis region are physically the same, ambiguities in the energy calibration due to contact potential differences are avoided. The ion beam energy and its spread are determined by fitting a Gaussian distribution to the retarding energy curve. The laboratory ion energies, E_{lab}, are converted to center-of-mass frame ion energies, $E_{c.m.}$, via the usual stationary target assumption[20]:

$$E_{c.m.} = E_{lab} \cdot m/(M+m), \tag{4}$$

where M is the ion mass and m is the target molecule mass. The precision of the determination of the energy zero is ± 0.01 eV lab. Based on comparisons with time-of-flight measurements of the ion energy[20] and considerations of possible systematic errors,[21] the overall accuracy in the energy determination is conservatively estimated to be within ± 0.1 eV lab [± 13, ± 18, and ± 22 meV c.m. for reactions (1), (2), and (3), respectively]. At very low ion energies, the slower ions in the ion beam energy distributions are

not transmitted through the octopole, which results in a narrowing of the ion energy distribution. The center-of-mass frame energies in the data plot are mean ion energies taking into account the truncation of the Gaussian beam distribution.[20]

$N^+(^3P)$ ion source

It is important to avoid contamination of the ion beam with metastable excited states of N^+. It has been shown[3] that the early differential scattering measurements[1,2,6] are flawed by the presence of excited N^+ in ion beams produced by electron impact ionization of N_2. High pressure dc discharge and microwave discharge sources also produce appreciable amounts (up to 10%) of excited state N^+ ions.[5,23]

For the experimental measurements reported herein, beams of ground state $N^+(^3P)$ are produced using a high pressure drift cell ion source. This source is modeled after the design of Bowers and co-workers[24] and is described in detail elsewhere.[21] He^+ ions produced by electron impact ionization are injected into a 2 cm long drift region which contains a relatively high pressure (100 to 500 mTorr) of N_2 gas. The dissociative charge transfer reaction

$$He^+ + N_2 \rightarrow N^+ + N + He, \quad \Delta H = -0.29 \text{ eV} \quad (5)$$

produces nitrogen ions only in the $N^+(^3P)$ ground state, since formation of excited state is endoergic.[26,27] Excited states could be formed by translationally hot He^+ ions, but are likely to be quenched by the further collisions with N_2.[25] The ions undergo numerous collisions with the bath gas while being drawn through the cell by a weak electric field (1 to 5 V cm^{-1}) towards an exit aperture. These collisions thermalize the ions translationally and internally.

The state composition of the N^+ ion beam is checked by monitoring the charge transfer reaction with hydrogen,[26]

$$N^+(^3P) + H_2 \rightarrow H_2^+ + N, \quad \Delta H = +0.9 \text{ eV}, \quad (6)$$

or the analogous reaction with deuterium at low energies. This reaction is endothermic for ground state $N^+(^3P)$, but is exothermic for the ^1D (1.9 eV), ^1S (4.0 eV), and higher excited states.[27] The H_2^+ charge transfer channel is absent below the 0.9 eV threshold for N^+ beams produced by the drift cell source. This confirms that only $N^+(^3P)$ is present in the ion beam. In contrast, N^+ produced by high energy electron impact on N_2 gives rise to a readily observable H_2^+ cross section at low energies.

Preliminary experiments on reactions (1), (2), and (3) were performed with two other ion source configurations. In one, the drift cell region is filled with N_2 gas and electrons are injected through the entrance aperture. N^+ and N_2^+ ions are formed by electron impact, but the electron energy is kept below the 42 eV threshold[26] for formation of N_2^{2+}, which would be passed by the initial mass analyzer at the same m/z setting as N^+. The observation of $(N_2)_n^+$ cluster ions up to at least $n = 3$ is evidence that the ions reach thermal equilibrium via collisions with the N_2 bath gas. In the other source configuration, ions initially produced by electron impact on N_2 are injected into the drift cell containing argon. Collisions with the Ar bath gas are relied upon to quench excited states of the N^+ ions as well as to thermalize the ions translationally.

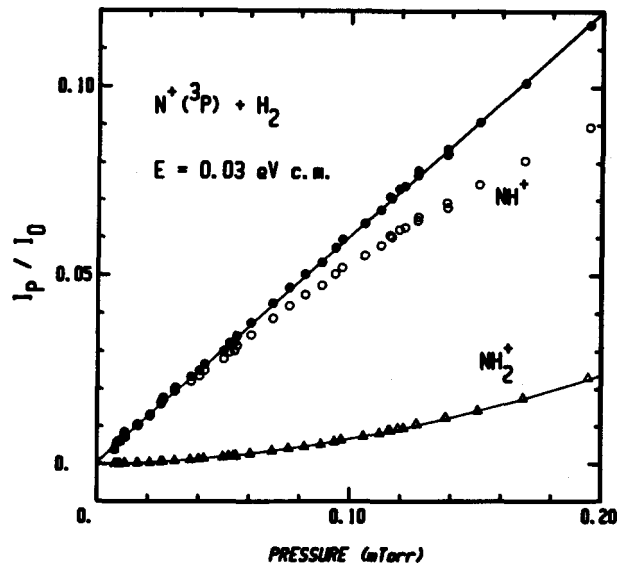

FIG. 1. Ratio of product ion intensity to the incident ion intensity I_p/I_0 as a function of the H_2 gas pressure for reaction (1) at an energy of 0.03 eV c.m. The solid circles are the sum of intensities of the primary product ion NH^+ (open circles), the secondary product ion NH_2^+ (open triangles), and minor secondary and tertiary products H_3^+ and NH_3^+ (not shown).

Experiments using these ion source arrangements were performed at different times over the course of a year. The three methods of making $N^+(^3P)$ gave identical results, within statistical uncertainties, both in the magnitude and relative behavior of the cross sections for reactions (1), (2), and (3). The He^+/N_2 source was used in the final set of experiments, for which full pressure dependence studies were performed.

Isotopic reagents

Commercially supplied H_2 and D_2, 99.99% purity, is used. HD gas is synthesized by standard methods[28] and has a purity of greater than 96%, as determined by mass spectrometric and by Raman spectroscopic analyses. The impurities are H_2 and D_2 in approximately equal amounts. No corrections for these impurities are applied to the data.

Pressure dependence

The pressure in the main reaction cell is generally kept low enough to ensure that multiple collisions are improbable. "Single collision" conditions are never strictly applicable since there is a finite probability of an incident ion encountering more than one neutral molecule along its path through the reaction cell. The probability of more than one collision increases with decreasing ion energy. The requirements for accurate cross section measurements are that (1) double collisions (either sequential or three body) do not contribute significantly to the product ion intensity and that (2) secondary reactions do not significantly reduce the product ion intensity. For most systems, these conditions are satisfied when the total attenuation of the ion beam is less than a few percent.

In the case of reactions (1), (2), and (3) at low energy, the following secondary and tertiary reactions can be signifi-

cant even at the low pressures normally used in the guided beam experiments[26,29,30]:

$$NH^+ + H_2 \rightarrow NH_2^+ + H, \quad \Delta H = -1.9\ \text{eV}, \quad (7a)$$

$$\rightarrow H_3^+ + N, \quad \Delta H = -6.2\ \text{eV}, \quad (7b)$$

$$NH_2^+ + H_2 \rightarrow NH_3^+ + H, \quad \Delta H = -1.1\ \text{eV}, \quad (8a)$$

$$\rightarrow H_3^+ + NH, \quad \Delta H = -3.3\ \text{eV}. \quad (8b)$$

The product ion intensities for reactions (1) and (7a) at $E_{c.m.} = 0.03$ eV as a function of pressure are shown in Fig. 1. The NH^+ primary product intensity is linearly dependent on pressure at low pressures as expected for a single collision process, but deviates at higher pressures due to depletion by the secondary reactions. The NH_2^+ secondary product intensity shows quadratic dependence on the H_2 pressure. The H_3^+ and NH_3^+ products (not shown) are an order of magnitude smaller in intensity than NH_2^+. These observations are consistent with the known behavior of reactions (7) and (8). At thermal energies, reaction (7) proceeds at the LGS collision rate and produces 85% NH_2^+ and 15% H_3^+.[31] The thermal rate for reaction (8a) is about 20% of the LGS limit and reaction (8b) is not observed.[31] The sum of the NH^+ primary product and the products of reactions (7) and (8), also shown in Fig. 1, has a linear dependence on pressure, indicating that there is no significant loss in total ion collection despite the large secondary reaction at higher pressures. The slope of this line, which is proportional to the reaction cross section,[20] is the same as the slope of NH^+ alone in the low pressure limit.

The secondary reactions are significantly only at low ion energies (<0.5 eV lab), for which the product ions have a long residence time in the interaction region as they drift through the octopole beam guide towards the detector. To obtain accurate cross sections, measurements are performed at a number of pressures from 0.004 to 0.1 mTorr (0.5 to 13 Pa) in the reaction cell. The cross sections are then extrapolated to zero pressure. For reactions (1) and (2), identical results are obtained at the higher pressures by summing the primary and secondary product intensities. This verifies that all products are collected. In some of the data analysis, cross sections obtained by summing the primary and secondary products are used as independent data sets for reactions (1) and (2). For the reaction with HD, however, mass overlap between isotopic variants of the products, in particular ND^+ and NH_2^+, prevents such a treatment. For reaction (3), therefore, only measurements directly extrapolated to zero pressure are used.

REACTION CROSS SECTIONS

Experimental cross sections for reactions (1), (2), and (3) are shown in Figs. 2, 3, and 4, respectively. The results shown have been extrapolated to zero reactant pressure as described above to eliminate the effect of secondary reactions. The cross sections are averages of several determinations at each energy.

Low energies

The collision cross sections predicted by the LGS model[16,32] for the ion–induced dipole potential are plotted in

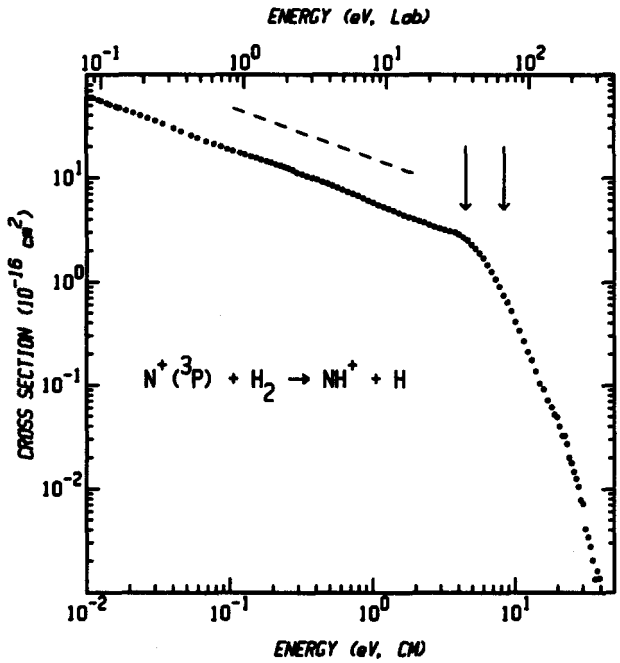

FIG. 2. Cross section for reaction (1) as a function of $N^+(^3P)$ ion kinetic energy in the laboratory frame (upper scale) and the center-of-mass frame (lower scale). Each solid circle represents an average of several determinations. The broken line gives the cross section predicted by the LGS model for ion–molecule reactions. The arrows indicate the 4.5 eV thermodynamic and 8.4 eV pairwise energy thresholds for product dissociation by process (10).

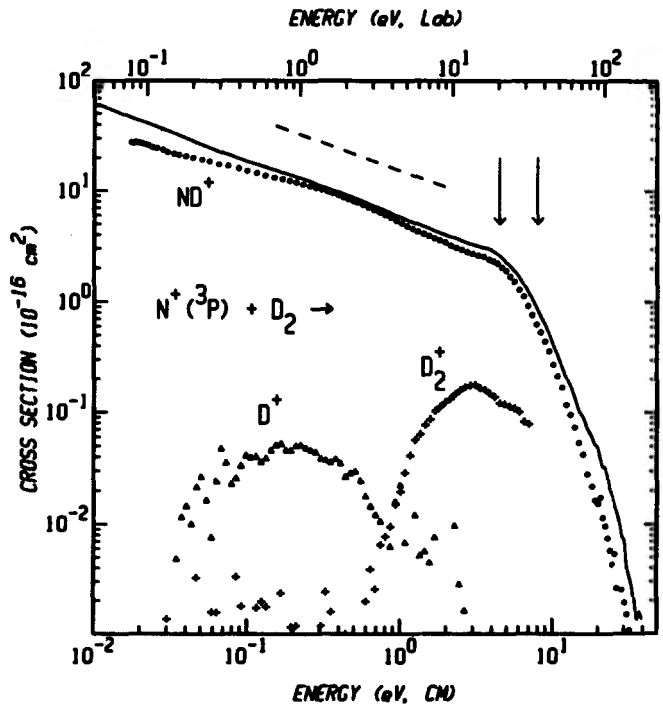

FIG. 3. Cross sections for reaction of $N^+(^3P)$ with D_2 as a function of the ion kinetic energy in the laboratory frame (upper scale) and the center-of-mass frame (lower scale). The results for formation of ND^+ (circles) represent the average of several determinations. Cross sections for formation of D^+ (triangles) and D_2^+ (crosses) are a single representative scan. The solid curve reproduces the experimental cross section for reaction (1) for comparison. The broken line gives the collision cross section according to the LGS model. The arrows indicate the 4.5 eV thermodynamic and 8.0 eV pairwise energy thresholds for product dissociation (see the text).

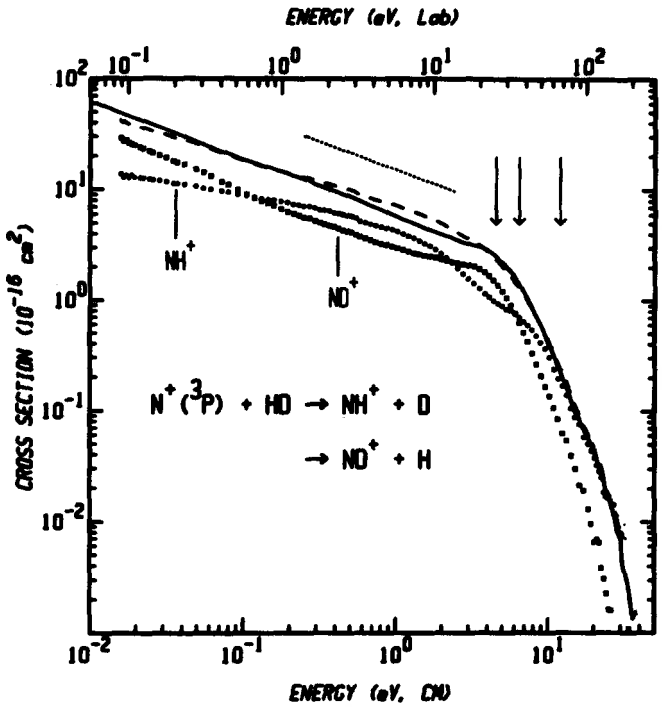

FIG. 4. Cross sections for reactions (3a) and (3b) as a function of the ion kinetic energy in the laboratory frame (upper scale) and the center-of-mass frame (lower scale). The cross section for formation of NH^+ is given by solid circles and the cross section for formation of ND^+ is given by open squares. The total reaction cross section, dashed line, is compared to the cross section for reaction (1), solid line. The LGS model collision cross section is shown by the dotted line. The arrows indicate the 4.5 eV thermodynamic threshold for product dissociation, the 6.4 eV pairwise dissociation threshold for the ND^+ product, and the 11.9 eV pairwise dissociation threshold for the NH^+ product (see the text).

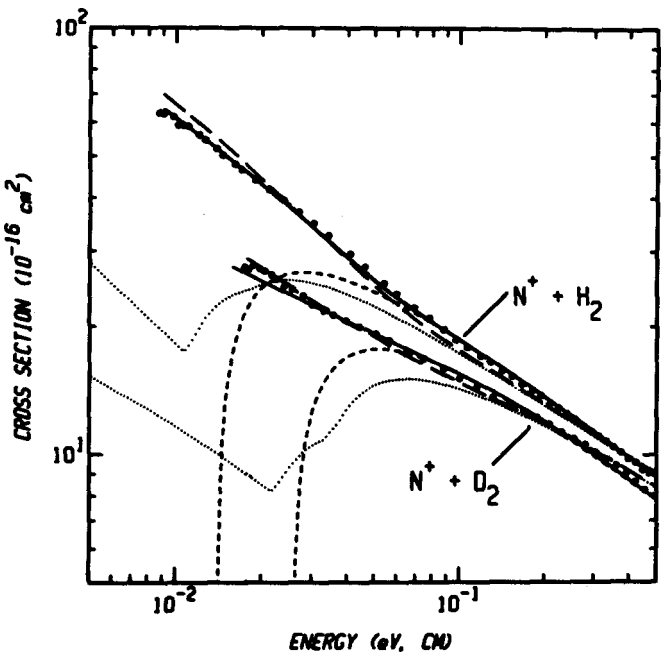

FIG. 5. Low energy behavior of the cross sections for reactions (1) and (2). The points reproduce the experimental data. The short dashed lines show the empirical model given by Eq. (12) with $n = 0.5$ and threshold energies given in Table II. The solid curves are the same functions convoluted over the experimental energy distributions for comparison with the data. The dotted lines are the phase space theory cross sections with the parameters listed in Table II. The broken lines show the convoluted versions of the PST cross sections.

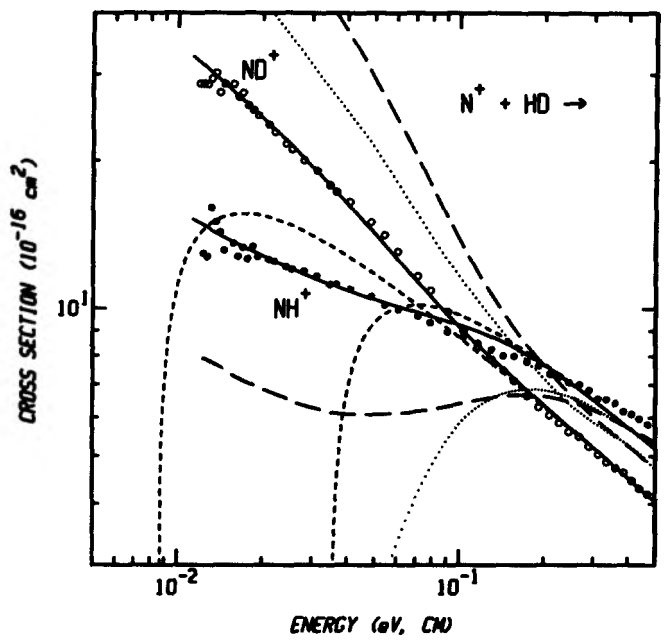

FIG. 6. Low energy behavior of the cross sections for reaction (3a), solid circles, and (3b), open circles. The short dashed lines show the empirical model given by Eq. (12) with $n = 0.5$ and threshold energies given in Table II. The solid curves are the same functions convoluted over the experimental energy distributions for comparison with the data. The dotted lines are the phase space theory cross sections with the parameters discussed in the text. The broken lines show the convoluted versions of the PST cross sections.

Figs. 2, 3, and 4 for comparison to experiment. In the low energy region, the energy dependence of the total cross sections is similar to the $\sigma(E) \propto E^{-1/2}$ behavior predicted by the LGS model. However, the magnitudes are smaller than the LGS model, ranging from 23% to 46% of σ_{LGS} below 0.5 eV.

The low-energy behavior of reactions (1), (2), (3a), and (3b) is compared on an expanded scale in Figs. 5 and 6. These plots show clear deviations among the various isotopic channels. The cross sections for reactions (2) and (3a) have a significantly smaller slope at low energies than reactions (1) and (3b). This behavior is attributable to the larger reaction endothermicities of reactions (2) and (3a) due to vibrational zero-point energy differences. According to the SIFDT study,[19] the reaction endothermicities at 300 K are 11 ± 3 meV, 34 ± 4 meV, 45 ± 6 meV, and <0 for reactions (1), (2), (3a), and (3b), respectively. Energy barriers of this magnitude are not observed as distinct thresholds in the apparent cross sections due to experimental energy broadening, but the deviations in the cross section behavior at low energies are clearly due to these differences in energetics. In a later section, the energy dependence of the cross sections is analyzed to obtain estimates of the reaction thresholds.

Intermediate energies

Above about 0.5 eV, the apparent cross sections for reactions (1) and (2) exhibit subtle changes in slopes (Figs. 2 and 3). The energy dependence of the cross sections from 0.5 to 3.5 eV is E^{-m} with $m = 0.54 \pm 0.01$ for reaction (1) and $m = 0.61 \pm 0.01$ for reaction (2). This decline is slightly

steeper than the $m = 0.5$ slope predicted by the LGS collision model, suggesting that the reactions become less efficient with increasing energy. Changes in behavior are also apparent in the cross sections for reactions (3a) and (3b) beginning about 1 eV. Below this energy, NH^+ is formed preferentially except at the lowest energies where the reactivity is dominated by the different endothermicities for the two channels. Above 1 eV, the fraction of NH^+ produced begins to decrease with increasing energy such that ND^+ is favored above 2.5 eV.

This behavior correlates with the onset of asymmetric scattering in the differential scattering measurements of Mahan and co-workers,[5] although these studies suggest that a long-lived NH_2^+ complex mechanism predominates below 2.0 eV. The different behavior above this energy was interpreted as indicating either an intermediate complex with a shorter lifetime or a more direct reaction mechanism.

A rationale for this change in behavior is provided by potential energy surface calculations.[10,13] This work shows that at low energies the $N^+ + H_2$ reactants can follow an adiabatic path to the 6 eV deep NH_2^+ ($^3B_1$–$^3A''$) potential well via an avoided crossing in C_s symmetry with the $^3A_2$–$^3A''$ surface, which is the only attractive surface at long range. At higher energies there is a high probability for transitions to the upper surface, i.e., diabatically going to NH_2^+ ($^3A_2$), which has a 2.6 eV potential well. An estimate[10] of the transition probabilities gives 0.53 at 0.5 eV, increasing to 0.73 at 1.0 eV, both for an expanded H–H distance of 3.5 bohr. If the H–H coordinate is further expanded to 4.0 bohr, the transition probabilities are greater than 90%. The relative probabilities of product formation from the $^3B_1$ and $^3A_2$ intermediates are unknown, but the present results suggest that trajectories which hop to the upper surface lead to products less often and react via a different mechanism than those trajectories which sample the NH_2^+ ($^3B_1$) well.

High energies

The cross sections for reactions (1), (2), and (3) begin decreasing more rapidly with increasing energy above about 4 eV. This decline correlates with the onset of NH^+ product dissociation. The lowest-energy dissociation process is dissociative charge transfer,

$$N^+(^3P) + H_2(^1\Sigma) \rightarrow [NH^+(^2\Pi) + H(^2S)] \rightarrow N(^4S) + H^+(^1S) + H(^2S), \quad (9)$$
$$\Delta H = 3.5 \text{ eV}.$$

However, this dissociation of $NH^+(^2\Pi)$ into the ground states of $N + H^+$ is spin forbidden. Indirect collision induced dissociation,

$$N^+(^3P) + H_2(^1\Sigma) \rightarrow [NH^+(^2\Pi) + H(^2S)] \rightarrow N^+(^3P) + H(^2S) + H(^2S), \quad (10)$$
$$\Delta H = 4.5 \text{ eV},$$

is the spin-allowed decomposition channel for $NH^+(^2\Pi)$. The total cross sections for reactions (1), (2), and (3) exhibit a definite break, the beginning of the high-energy decay region, which occurs at the threshold energy of process (10) rather than process (9), as illustrated by arrows at 4.5 eV in Figs. 2, 3, and 4. This conclusion is substantiated using a statistical model for the high energy decay which has been described elsewhere.[33] Reasonable fits are obtained for a diatomic dissociation energy $D = 4.5$, but not for $D = 3.5$ eV.[34] This strongly implies that process (10) is the predominant dissociation process, at least near the thermodynamic threshold, and hence that spin is conserved. At higher energies, dissociation to ground state $N(^4S) + H^+(^1S)$ may become spin allowed via excited NH^+ intermediates.

For direct impulsive reaction mechanisms, product dissociation cannot occur at the thermodynamic threshold, but rather is shifted to higher energies because some energy is tied up in product translation. The effective interaction energy for a mechanism in which the N^+ interacts in a pairwise impulsive fashion with only one hydrogen or deuterium atom has been derived previously.[35] The effective pairwise energy threshold, E_S, for dissociation of the putative NH^+ or ND^+ product via process (9) [or via process (10), in brackets] is 6.6 eV [8.4 eV] for $N^+ + H_2$ and 6.3 eV [8.0 eV] for $N^+ + D_2$. For the reaction with HD, $E_S = 9.4$ eV [11.9 eV] for $NH^+ + D$ intermediates and $E_S = 5.0$ eV [6.4 eV] for $ND^+ + H$. The lower dissociation energy for ND^+ products manifests itself by an earlier falloff for reaction (3b) compared to reaction (3a), Fig. 4, giving rise to a very strong intramolecular isotope effect in the high energy region. This behavior supports the view that the reaction mechanism involves direct, impulsive behavior at these high energies.

The familiar spectator stripping (SS) model[36] is a special case of a pairwise impulsive process. The pairwise dissociation thresholds, E_S, are identical to the SS critical energies, above which diatomic products cannot be formed because they have too much internal energy and are unstable to dissociation. The SS critical energies do not correlate with any sharp feature in the reaction cross sections, but rather fall in the middle of the high-energy decay region (Figs. 2, 3, and 4). Some blurring of a sharp dissociation could result if both process (9) and process (10) occur in this region. However, stable diatomic products are observed far above the critical energies. This indicates that more of the available energy is distributed into product translation than in the spectator stripping model. Conversely, the decline in the reaction cross sections before the pairwise dissociation thresholds indicate that more energy can go into internal modes than predicted by the pairwise impulsive model.

The foregoing interpretation is consistent with the differential scattering results[4,5] which indicate that reaction (1) becomes increasingly direct at high energies, evolving from symmetric scattering at low energies to peaking at the spectator stripping velocity at collision energies just below the critical energy. At energies above the spectator stripping critical energy, the spectator stripping peak diminishes as expected and is replaced by sideways scattering. However, substantial wide-angle scattering is observed throughout the energy range examined. This indicates a wide distribution of energies in translational and internal degrees of freedom.

The energy dependence of the cross sections in the falloff region, 7 to 20 eV, is $E^{-3.2\pm0.1}$ for reaction (1) and $E^{-3.8\pm0.2}$ for reaction (2). Above about 20 eV, the cross

sections decline even more rapidly. At these energies, reactions (1) and (2) have an energy dependence of $\sigma(E) \propto E^{-5.5\pm0.2}$. This behavior suggests that at very high energies, stable products cannot be formed by any mechanism and hence the cross section rapidly goes to zero. The $E^{-5.5}$ energy dependence matches that derived by Bates *et al.*[37] for an impulsive capture model, although their calculations apply to kilovolt or higher ion energies.

Other product channels

Figure 3 also presents cross sections for additional product channels for $N^+(^3P) + D_2$: formation of D_2^+ by charge transfer, reaction (6), and formation of D^+, either by dissociative charge transfer, reaction (9), or by the reaction[26,30]

$$N^+(^3P) + D_2 \rightarrow D^+ + ND, \quad \Delta H = 0.14 \pm 0.06 \text{ eV}. \quad (11)$$

Measurement of these reaction channels with the guided beam apparatus is difficult, for the following reasons. Since the D^+ and D_2^+ product channels do not include the heavy nitrogen atom in the ionic product, backwards scattering in the lab frame is kinematically possible. Collection of backscattered products can be achieved in the guided beam technique, but requires special precautions (as described previously[20]) which were not taken for the data presented in Fig. 3. Low-mass products may also be subject to mass discrimination in the final quadrupole mass spectrometer. The data shown are not corrected for mass discrimination. At high energies (> 20 eV lab), products from charge transfer reactions are not efficiently transmitted through the quadrupole due to their small laboratory kinetic energies.[20] For these reasons, the cross sections for reactions (6), (9), and (11) in Fig. 3 may have low absolute magnitudes and should be considered qualitative. Results are presented only for the deuterium reactions since the quadrupole resolution and transmission problems are more severe for H^+ and H_2^+ products. The pressure dependence of the product intensities confirms that they are primary reaction products and are not due to secondary collisions. The D^+ and D_2^+ data shown in Fig. 3 represent a single representative energy scan, while the ND^+ results are averaged from several determinations and therefore have less scatter.

The D^+ and D_2^+ product channels are of minor importance compared to formation of ND^+ over the energy range covered here. The D_2^+ charge transfer product exhibits an apparent threshold which coincides with the 0.9 eV endothermicity for the reaction with ground state $N^+(^3P)$ ions. The scattered data at lower energies are base line noise. The absence of D_2^+ at low energies confirms that the ion beam is not contaminated with excited states of N^+. The cross section rises to at least 5% of the cross section of reaction (2) at 3 to 4 eV. The apparent decline at higher energies is probably due to the detection problems discussed above. Mahan and Ruska[4] inferred from the low intensity of nonreactive scattering and the observation of slow ionic products that charge transfer is the dominant reaction channel in the 6 to 15 eV range. The charge transfer cross section at kilovolt ion energies is $(3\text{–}4)\times10^{-16}$ cm^2 for $N^+ + H_2$.[38]

Atomic D^+ ions are observed well below the 3.5 eV threshold for dissociative charge transfer, reaction (9), indicating that the neutral product must be diatomic ND, reaction (11). The D^+ cross section exhibits an apparent threshold which, considering the effects of the experimental energy broadening, is consistent with the 0.14 ± 0.06 eV endothermicity derived from literature thermochemistry.[26,30,39] Due to the qualitative nature of the data, no attempt was made to determine the experimental threshold energy quantitatively. D^+ is not observed at high energies in the falloff region for the ND^+ cross section. This is another indication that the main dissociation channel is $N^+ + D + D$.

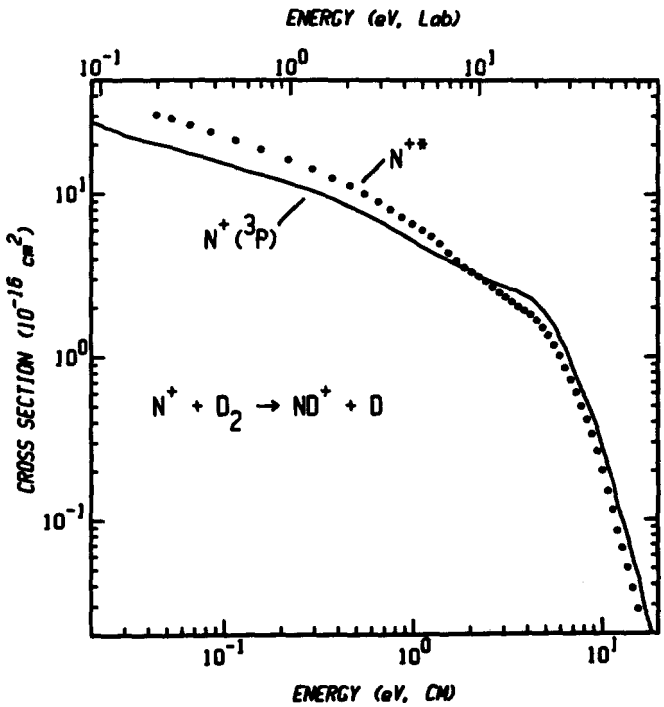

FIG. 7. Cross sections for reaction (2) with ground state $N^+(^3P)$ ions (line) are compared with the results for N^+ ions formed by electron impact at 160 eV electron energy (points).

Excited state reactant ions

Experiments were also performed with N^+ ions formed directly by electron impact ionization without undergoing collisions in the drift cell. At high electron energies, electron impact is expected to make an appreciable fraction of metastable excited states of N^+ and also to produce N_2^{2+}, which is passed by the initial magnetic momentum analyzer along with N^+.

The cross sections of reaction (2) for $N^+(^3P)$ produced by the drift cell ion source and for N^+ produced by 160 eV electron impact are compared in Fig. 7. Experiments performed with ions made with an electron energy of 38 eV gave cross sections intermediate in magnitude between the ground state $N^+(^3P)$ and the 160 eV electron impact N^+ results shown in Fig. 7. At low energies, the cross section for the beam containing excited states is up to 50% larger than for ground state ions. If we assume that excited states react with a cross section given by the LGS collision model as an upper limit, we can estimate a lower limit of about 30% for the fraction of reactive excited states in the ion beam. This is consistent with Mahan and co-workers,[5,23] who found popu-

lations of roughly 50% N^{+*} and 10% N_2^{2+} from 160 eV electron impact on N_2. At high energies, the cross section for the mixed state beam declines with an energy dependence similar to $N^+(^3P)$, but the cross section magnitude is slightly smaller above 3 eV. The lower reactivity of the excited states in the high energy region is consistent with a lower threshold energy for product dissociation for excited reactants, analogous to processes (9) and (10).

The large difference between the apparent cross sections for the ion beam with excited states and the cross sections for ground state $N^+(^3P)$ demonstrates the importance of characterizing the internal energy of the reactant ions. The present results confirm the inference of Mahan and co-workers[5] that the reaction cross section of the excited state(s) is much larger than that of the ground state in this energy region. For this reason, excited states dominate the differential scattering at low energies whenever they are present in substantial quantities.

THRESHOLD BEHAVIOR

The threshold behavior of the cross sections for reactions (1), (2), and (3) is obscured by experimental energy broadening. In this section, procedures to extract threshold energies from the experimental data are described.

Energy broadening

The random thermal motion of the target gas and the ion beam energy spread create a distribution of interaction energies for each nominal ion energy. The broadening is especially severe for energies $E<0.1$ eV c.m., where thresholds in the microscopic cross sections for reactions (1), (2), and (3) are expected. Mathematical derivations of the effect of the energy distributions on the observed cross sections have been presented previously.[20,22,40,41]

The broadening effect due to reactant gas thermal motion at low ion energies may be conceptually understood as follows. For very small ion beam velocities, the relative energy distribution is determined primarily by the Maxwell–Boltzmann distribution of the thermal target gas. At 300 K, the thermal distribution extends to energies above the thresholds for reactions (1), (2), and (3). Therefore, ions passing through the gas cell with little or no energy will react at a constant, near-thermal rate. The extent of reaction, then, is proportional to the residence time of the ions in the interaction region. The residence time is given by Q/v, where Q is the path length and v is the ion velocity. Since $Q/v \propto E^{-1/2}$, the apparent cross sections tend toward the behavior $\sigma(E) \propto E^{-1/2}$ as $E \rightarrow 0$, regardless of the functional form of the true cross section.

Broadening from the ion beam energy spread is negligible compared to broadening from target gas motion at moderate and high energies, but is significant at low energies where the ion energy spread is large relative to the mean ion energy. At very low energies, slow ions are truncated from the Gaussian energy distribution, resulting in a narrowing distribution as the energy is decreased. These effects are described in detail elsewhere.[20,22,42]

Despite the extent of energy broadening in this case, information about the behavior of the true cross sections can be inferred from the experimental cross sections. Methods for extracting the true cross sections from the energy-broadened observed cross sections have been treated previously.[20,22] This involves forward convolution of a model cross section over the experimental energy distribution for comparison with the data. The model cross section is then adjusted to achieve the best fit to the experimental data. The true cross section cannot be uniquely determined, however, and prior assumptions about the form of the true cross section are necessary. In the following, we use several empirical

TABLE II. Cross section model parameters and threshold energies.[a]

		Cross section form $\sigma(E)$				
Reactant	$\Delta G(0)$[b]	$\sigma_0\frac{(E-E_T)^{1/2}}{E}$	$\sigma_0\frac{(E-E_T)^n}{E}$	$\sigma_0\frac{[E-E_T+E(J)]^{1/2}}{E}$	$\sigma_0\frac{[E-E_T+E(J)]^{1/2}}{E+E(J)}$	PST[c]
(1)	−82.6	$E_T=14.0$ $\sigma_0=6.34$	$E_T=15.4$ $\sigma_0=6.11$ $n=0.48$	$E_T=34.1$ $\sigma_0=6.47$	$E_T=23.4$ $\sigma_0=6.48$	$\Delta E_0=18.2$ $\sigma_0=2.69$
(2)	−55.0	$E_T=25.8$ $\sigma_0=5.70$	$E_T=21.9$ $\sigma_0=6.14$ $n=0.56$	$E_T=53.2$ $\sigma_0=5.87$	$E_T=45.3$ $\sigma_0=5.82$	$\Delta E_0=36.7$ $\sigma_0=2.44$
(3a)	−47.1	$E_T=34.8$ $\sigma_0=3.79$	$E_T=27.4$ $\sigma_0=4.44$ $n=0.61$	$E_T=68.3$ $\sigma_0=4.01$	$E_T=62.7$ $\sigma_0=4.18$	
(3b)	−97.1	$E_T=8.5$ $\sigma_0=2.88$	$E_T=10.7$ $\sigma_0=2.73$ $n=0.47$	$E_T=23.9$ $\sigma_0=2.87$	$E_T=19.1$ $\sigma_0=2.95$	
ΔE_e[d]		116 ± 12[e]	114 ± 16[e]	115 ± 5	108 ± 7	96 ± 6

[a] Parameters optimized as described in the text. All energies in meV units.
[b] Change in vibrational zero-point energy (meV), from data in Table III.
[c] Phase space theory.
[d] Vibrationless change in energy, $\Delta E_e = E_T - \Delta G(0)$. Values are the averages for reactions (1), (2), (3a), and (3b), $\pm$ 1 standard deviation.
[e] Corrected to 0 K by adding the mean rotational energy of hydrogen reactant (see the text).

TABLE III. Molecular constants.

Species	D_0° (eV)	ω_e (cm^{-1})	$\omega_e x_e$ (cm^{-1})	B_e (cm^{-1})	$G(0)$[a]
$NH^+(X^2\Pi)$	3.51 ± 0.03[b]	3038[c]	58[c]	15.67[c]	0.1865
$ND^+(X^2\Pi)$	3.56 ± 0.03[b]	2218[c]	31[c]	8.35[c]	0.1365
$H_2(^1\Sigma^+)$	4.4781[d]	4401.2[d]	121.33[d]	60.853[d]	0.2691
$HD(^1\Sigma^+)$	4.5138[d]	3813.15[d]	91.65[d]	45.66[d]	0.2336
$D_2(^1\Sigma^+)$	4.5563[d]	3115.50[d]	61.82[d]	30.443[d]	0.1915

[a] Zero-point vibrational energy, $G(0) = \omega_e/2 - \omega_e x_e/4$, in eV.
[b] This work.
[c] I. Kusunoki and Ch. Ottinger, J. Chem. Phys. **80**, 1872 (1984).
[d] K. P. Huber and G. Herzberg, *Constants of Diatomic Molecules* (Van Nostrand Reinhold, New York, 1979).

cross section models and a phase space theory model to analyze the low energy cross sections.

Power law threshold model

An empirical power law threshold form has proven useful for modeling the behavior of a number of endothermic ion–molecule reactions.[21,33,35,43] This function is given by

$$\sigma(E) = \sigma_0 \cdot (E - E_T)^n / E^m \quad \text{if } E > E_T,$$
$$\sigma(E) = 0 \quad \text{if } E \leqslant E_T, \tag{12}$$

where E is the relative kinetic energy of the reactants, E_T is the threshold energy, σ_0 is an energy-independent scaling factor, and n and m are either derived from a theoretical model or are adjustable parameters. A model[44] for endoergic ion–molecule reactions based on the long range ion–induced dipole potential predicts $n = 0.5$ and $m = 1$. A variant of this model, in which n is allowed to vary, gives reasonable fits to the data for the related $C^+ + H_2 \rightarrow CH^+ + H$ reaction, which has a known threshold energy of ~ 0.4 eV.[21] The hard-sphere line-of-centers model,[45] $n = m = 1$, often is found to describe the behavior of endothermic reactions with higher thresholds, for example, $Si^+ + H_2 \rightarrow SiH^+ + H$, $E_T \approx 1.19$ eV.[46]

Equation (12) was optimized to fit the cross section data up to 0.5 eV with a fixed value of $m = 1$ and n either fixed at 0.5 or optimized as an adjustable parameter. The results are given in Table II. The $n = 0.5$ model cross section and its convolution is compared to the data in Figs. 5 and 6. Note that when n is allowed to vary, it maintains values from 0.47 to 0.61, near the ion–induced dipole model of $n = 0.5$, for all four reactions. The slope of the experimental cross sections above about 0.1 eV requires that $(n - m) \approx -0.5$ in Eq. (12). This tends to exclude values of n and m which greatly differ from the ion–induced dipole model.

Considering the uncertainties of the fitting procedure and the variance of values obtained from independent sets of data, we estimate the uncertainties for the threshold energies given in Table II are ± 5 meV. This does not include systematic errors due to the assumption of a particular cross section model or errors in the experimental energy calibration. The threshold values obtained with the $n = 0.5$, $m = 1$ model agree within combined uncertainties with the threshold obtained when n is allowed to vary, Table II. The threshold values are also in reasonable agreement with the uncorrected activation energies obtained from the SIFDT[19] experiments: 13 ± 3 meV for reaction (1), 34 ± 4 meV for reaction (2), and 45 ± 6 meV for reaction (3a). The SIFDT results indicate that reaction (3b) is slightly exothermic, while we obtain a small positive threshold energy.

Vibrational zero-point energy

In order to compare the threshold energies obtained for the various isotopic reactions, we define a vibrationless energy change given by $\Delta E_e = E_T - \Delta G(0)$, where $\Delta G(0)$ is the change in diatomic zero point vibrational energies, $G(0)$,[47] for the reaction. The diatomic vibrational frequencies are tabulated in Table III and $\Delta G(0)$ is listed in Table II. If the variation in threshold energies for reactions (1), (2), (3a), and (3b) is due solely to the difference in zero point energies, ΔE_e should have the same value for all four reactions. The average of the ΔE_e values for the four reactions are 91 ± 12 meV for the fits with $n = 0.5$ and 89 ± 16 meV with n variable. The error limits are one standard deviation. Treating the SIFDT results[19] for reactions (1), (2), and (3a) in a similar way yields $\Delta E_e = 92 \pm 8$ meV, in good agreement with our result.

The standard deviations of the ΔE_e values provide an indication of how well the empirical threshold values follow the difference in zero point energies. Based on the ± 5 meV uncertainty in the individual E_T values, the propagated error in the average value of ΔE_e is ± 2.5 meV. Thus, the ± 12 and ± 16 meV observed standard deviations of the values of ΔE_e are larger than that expected due to statistical error. This indicates that the variation of the E_T values, as derived for this form of the model cross section, does not exactly correspond to the zero point energy differences.

Rotational energy

The preceding analysis ignores the hydrogen reactant rotational energy. As a first approximation, one can correct ΔE_e for the reactant rotational energy by adding in the mean rotational energy available under the experimental conditions (~ 0.025 eV at 305 K). The resulting corrected values for ΔE_e are shown in Table II. This correction assumes that (1) rotational energy can drive the reaction as efficiently as translational energy and that (2) the rotational energy may be treated in an average fashion, rather than for individual rotational states. The first assumption will be discussed below. The second approximation is questionable since the hydrogen rotational energy spacings are of the same order of magnitude as the reaction endothermicities. Moreover, at

305 K some of the populated rotational states have sufficient energy to make the reaction with N^+ exothermic.

A better treatment of rotational energy is given by an explicit sum of Eq. (12) over the individual rotational states:

$$\sigma(E) = \sum_J f(J)\cdot\sigma(E,J), \tag{13a}$$

where

$$\sigma(E,J) = \sigma_0\cdot[E - E_T + E_r(J)]^{0.5}/E \quad \text{if } E > E_T - E_r(J) > 0, \tag{13b}$$

$$\sigma(E,J) = 0 \quad \text{if } E_T - E_r(J) \geq E > 0, \tag{13c}$$

$$\sigma(E,J) = \sigma_0\cdot E^{-0.5} \quad \text{if } E_T - E_r(J) \leq 0, \tag{13d}$$

$f(J)$ is the fractional population[48] of rotational level J, and $E_r(J) = B_e J(J+1)$ is the rotational energy. The H_2, HD, and D_2 rotational constants, B_e, are listed in Table III. Equation (13d) makes the assumption that if the reaction is exothermic due to rotational energy, then the cross section is proportional to the collision cross section according to the LGS model. Only the $n = 0.5$, $m = 1$ form of the power law model cross section is used for simplicity and because similar results are obtained for Eq. (12) with either $n = 0.5$ or n variable.

Optimized values of E_T from fits of Eq. (13) to the data are presented in Table II. The average value for ΔE_e corresponds quite closely with those obtained by fitting Eq. (12) and correcting it by the mean rotational energy. This lends support for use of the simpler form.[49] The spread in the ΔE_e values is given by a standard deviation of 5 meV, which is smaller than for the fits to Eq. (12) and indicates that the derived threshold energies follow variations in $\Delta G(0)$ more closely. This suggests that the explicit treatment of the rotational energy levels in Eq. (13) more accurately models the energy dependence of the cross sections for the four reactions.

An alternate model replaces the relative kinetic energy E in the denominator of Eq. (13b) with the total energy $[E + E_r(J)]$. Some theoretical treatments support this form of the cross section.[50] The threshold energies obtained using this form of the cross section are also given in Table II. The threshold values are systematically lower than those obtained with the unmodified form of Eq. (13), leading to a ΔE_e value which is about 7 meV lower. It is not clear which of these two approaches is better from a theoretical standpoint for this system.

All four empirical models give similar values for ΔE_e after correction for the rotational energy, Table II. The assumption that rotational energy is completely available to drive the reaction, however, is faulty. Conservation of total angular momentum requires that the angular momentum due to rotationally excited reactants be matched in the products either as rotation of the NH^+ or ND^+ product or as orbital angular momentum of the products. Either way, some of the total energy of reactants will be tied up as rotational energy in the products and cannot be used to drive the reaction. Therefore, the effective threshold energy for $J > 0$ is expected to be slightly higher than the value obtained by requiring only that total energy is conserved.

PHASE SPACE THEORY

A more sophisticated treatment of rotational energy requires a model which explicitly conserves both energy and total angular momentum. Phase space theory[51,52] is a statistical model which does this. Its basic assumption is that there is a region of strong interaction of the reactants from which the system decomposes statistically into all accessible reactant and product states. The $N^+ + H_2$ system should be a good candidate for PST since the deep NH_2^+ potential well can support a long-lived intermediate. Differential scattering measurements indicate that the intermediate lasts for at least several vibrational periods and perhaps a rotational period.[5] We recently applied a semiempirical form of classical phase space theory[53,54] to the $C^+ + H_2$ system.[55] The same methods are used here. In the semiempirical form of PST, the reaction endothermicity is treated as an adjustable parameter. In addition, a scaling factor is used to compensate for the experimental uncertainty in the absolute magnitudes of the cross sections. Molecular constants required as input to the PST program are tabulated in Table III.

Following the method of Herbst and Knudson,[56] electronic degeneracy factors are used to specify which of the reactant and product electronic surfaces are accessible to the complex. The electronic state correlations of Mahan and coworkers[5] and the theoretical potential energy surface calculations[9,10,13] indicate which surfaces are accessible. For reactants, only one of the three triply degenerate surfaces in the entrance channel leads to the NH_2^+ intermediate without an energy barrier. The product channel has one triply degenerate accessible surface.[57]

The results of the classical phase space theory calculations for reactions (1) and (2) are presented in Fig. 5 and Table II. We find a threshold energy for $J = 0$ of 18 ± 5 meV for reaction (1) and 37 ± 5 for reaction (2). These give reasonable fits to the experimental data, as shown in Fig. 5, although the fits are not as good as for the empirical models. The ΔE_e value obtained from these two PST fits is 96 ± 6 meV, that is, 10 to 20 meV lower than those obtained from the empirical cross section models. This is expected because not all of the rotational energy is available to drive the reaction. Therefore, the endoergicity used in the PST model must be lower to compensate. To fit the data, the magnitudes of the PST cross sections must be scaled up by factors of $\sigma_0 = 2.69$ and $\sigma_0 = 2.44$ for reactions (1) and (2), respectively.

For reaction (3), no value for the reaction endothermicity in PST adequately reproduces the experimental cross sections for both the NH^+ and ND^+ channels. Figure 6 compares the experimental cross sections for reactions (3a) and (3b) to a PST calculation using activation energies based on $\Delta E_e = 96$, as obtained from reactions (1) and (2), and $\sigma_0 = 2.80$. The PST cross sections are qualitatively similar to the experiment, but the isotopic branching ratio clearly does not match the data quantitatively. Work on other systems ($C^+ + HD$,[55] $V^+ + HD$,[58] $Si^+ + HD$[59]) has shown that PST is generally less successful in describing isotope effects than in reproducing the energy dependence of the total cross sections. The deviation from experiment is rather extreme in this case; therefore, no thermochemical informa-

tion for the HD reaction can be obtained using semiempirical PST. Furthermore, the discrepancies for reaction (3) mean that the PST results for reactions (1) and (2) can be called into question.

The partial failure of PST could be attributed to nonstatistical behavior (i.e., dynamical effects), despite the expectation of statistical behavior for this system at low energies. However, the culprit could also be deficiencies of *classical* PST, where the rotational density of states for each channel is treated as a continuous classical distribution. Classical PST was shown to give nearly identical results as the quantum version for the $C^+ + H_2$ reaction.[53] For the $N^+ + H_2$ reaction, however, the rotational levels of the reactants and products have energy spacings which are of the same order of magnitude as the endoergicity. Therefore, the statistical decomposition of the NH_2^+ intermediate may depend in a critical way on the availability of the discrete rotational levels of products or reactants. This may affect the absolute magnitudes of the PST cross sections as well as the isotopic branching.

For similar reasons, the treatment of nuclear spin statistics in the PST[60] may be important for this system. If the nuclear spins are "frozen" during the reactions, some rotational energy levels of *para* and *ortho* hydrogen in the $N^+ + H_2$ channel will not be available upon decomposition of the intermediate. For other ion–molecule systems studied, it is not important whether nuclear spins are frozen or are fully coupled to other angular momenta in the phase space calculations.[53,60] This system would be an interesting case for the treatment of internal rotation and nuclear spin in quantum mechanical PST.

REACTION RATES

Direct comparison of our cross sections, $\sigma(E_{c.m.})$, to the SIFDT hyperthermal rate measurements, $k(E)$, and the thermal rates, $k(T)$, is not possible because of the different translational and internal energy distributions in the various experiments. In principle, the microscopic cross sections can be integrated over the energy distributions under the conditions of each experiment to reproduce the data. In this section, we use the inferred forms of the true cross sections, Table II, to obtain reaction rates for comparison to the previous experiments.

Thermal reaction rates may be obtained by integrating the cross sections over a Maxwell–Boltzmann distribution of translational energies.[20,21] For this purpose, the true unconvoluted cross sections must be used rather than the energy-broadened observed cross sections. Therefore, the accuracy of the derived reaction rates depends on our ability to determine the true cross sections. Averaging the rates based on each of the empirical cross section models described above, we obtain the following 300 K rate coefficients: $k_1 = 3.9 \pm 0.8$, $k_2 = 1.7 \pm 0.4$, and $k_3 = 2.7 \pm 0.6$ (34% NH^+/66% ND^+), all in units of 10^{-10} cm^3 s^{-1}. Good agreement with other recent determinations is obtained for k_1, Table I. Adams and Smith[19] measured 300 K rates for the other isotopic reactions also, obtaining $k_2 = 1.3 \pm 0.3$ and $k_3 = 3.5 \pm 0.9$.[61] These agree with the present results within the uncertainties. However, Adams and Smith obtain a branching ratio of 15% NH^+/85% ND^+ for reaction (3), i.e., favoring ND^+ production more than our result. An error in favor of ND^+ could occur due to the fast secondary reaction $NH^+ + HD \rightarrow NH_2^+ + D$, since NH_2^+ and ND^+ are detected at the same mass. In the present experiments, careful extrapolation of the cross sections for each channel to zero pressure eliminates this problem.

To obtain rates at low temperatures, the hydrogen rotation state population must be considered as well as the translational energy distribution. Under the conditions of the gas jet experiment,[17] rotational states are cooled to the reaction temperature, but with a normal 3:1 population of *ortho* to *para* hydrogen. In the low temperature ion trap experiment,[18] partial *ortho/para* equilibration could occur via exchange reactions on the walls of the inlet system.[62] For comparison to these results, we calculate the phase space theory rate constant at 10 K for both normal and equilibrium hydrogen. Using the $\Delta E_0 = 18.2$ meV value obtained by fitting PST to the cross section data, we obtain $k_1(10\,\mathrm{K}) = 7.3 \times 10^{-20}$ cm^3 s^{-1} for equilibrium hydrogen (virtually all $J = 0$) and $k_1(10\,\mathrm{K}) = 4.3 \times 10^{-16}$ cm^3 s^{-1} for normal hydrogen. Even the normal hydrogen rate is several orders of magnitude smaller than the rates obtained in the gas jet, $\sim 6 \times 10^{-12}$ cm^3 s^{-1},[17] and the ion trap, $\sim 1 \times 10^{-13}$ cm^3 s^{-1}.[18,63] To match the 10 K rates using PST, the reaction endothermicity must be lowered to $\Delta E_0 \approx 10$ meV for the gas jet rate and $\Delta E_0 \approx 13$ meV for the ion trap rate (both for normal hydrogen). Differences of only a few millielectron volts in the reaction endothermicity produces enormous changes in the 10 K rate constant, mainly due to the Boltzmann factor $\exp(-\Delta E/k_B T)$. Under the present experimental conditions, the cross sections are much less sensitive to ΔE_0, such that it is very difficult to extrapolate the results to low temperatures. Our data are consistent with the low temperature rate measurements within the experimental uncertainty of ΔE_0. A further uncertainty in this comparison is that the deficiencies of classical PST, discussed above, may be exacerbated at low temperatures and thus may affect the comparisons made here.

Next, we wish to compare the present results to the energy dependent rate measured by the SIFDT technique.[19] The ion translational energy distributions under the conditions of the SIFDT experiment are not easily characterized.[64] As a crude but reasonable approximation for low drift velocities, we use the energy distribution for monoenergetic ions (zero temperature) passing through a Maxwell–Boltzmann distribution of neutral molecules. The convolution function for this distribution has been given by Chantry.[40] It also corresponds to the energy distribution in beam/gas experiments for a monoenergetic ion beam. For comparison to the SIFDT results, we first convolute one of the model cross sections from Table II, then convert the resulting effective cross section into a phenomenological rate as a function of the mean interaction energy, $k(\langle E \rangle)$, as described previously,[20] and finally present the data in the form of a pseudo-Arrhenius plot, $\ln k$ vs $1/\langle E \rangle$, as given by Adams and Smith[19] for the SIFDT results. The results for Eq. (12) with $n = 0.5$ and E_T values from Table II are shown in Fig. 8. The other fits to the cross section data yield pseudo-Arrhenius

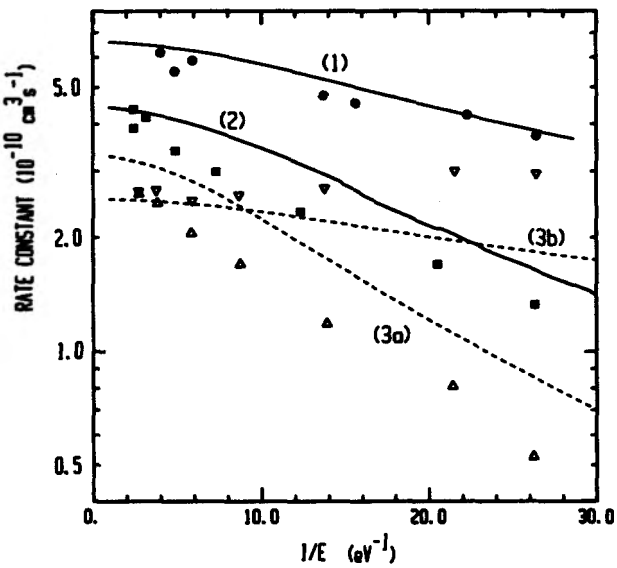

FIG. 8. Pseudo-Arrhenius plot of the phenomenological rate constants as a function of the inverse mean interaction energy. The curves show the empirical cross section model, Eq. (12) with $n = 0.5$ and threshold energies given in Table II, convoluted over the experimental energy distribution in the limit of monoenergetic ions. Solid curves show reactions (1) and (2); dashed curves show reactions (3a) and (3b). These curves are compared with the hyperthermal rate data from selected-ion flow/drift tube studies of Adams and Smith (Ref. 19): solid circles, reaction (1); solid squares, reaction (2); upright open triangles, reaction (3a); and inverted open triangles, reaction (3b).

plots (not shown) which have similar average slopes. The slopes of the lines match the SIFDT data reasonably well for reactions (1), (2), and (3a). The magnitude for the H_2 reaction also matches very well, and is within the experimental uncertainty for reactions (2) and (3a). The only qualitative discrepancy is that our plot for reaction (3b) has negative slope, corresponding to a positive activation energy, while the SIFDT data has a zero or slightly positive slope, which was interpreted as meaning the reaction is slightly exoergic. It is not clear whether this discrepancy can be explained by the different energy distributions for the two experiments. Since the threshold energy for reaction (3b) is very small, it is possible that a high energy component in the ion energy distribution could increase the rate constant in the SIFDT experiment. It is also possible that our deconvolution procedure overestimates the threshold.

The slopes of the pseudo-Arrhenius plots were used to derive activation energies from the SIFDT results.[19] In the pseudo-Arrhenius analysis, the mean interaction energy is converted to an effective translational temperature using the expression $\langle E \rangle = (3/2)k_B T_{\text{eff}}$. The activation energy is taken as the derivative $E_a' = -(2/3)\cdot d(\ln k)/d(1/\langle E \rangle)$. This is to be compared to the true Arrhenius activation energy $E_a = -d(\ln k)/d(1/k_B T)$. Since the interaction energy distributions are not thermal, either in ion beam experiments or in flow/drift experiments, this treatment is not exact. The pseudo-Arrhenius approach is valid only to the extent that changing the ion energy approximates a change in the reaction temperature, which may be the case for very small accelerations of the ions through the Maxwell–Boltzmann distribution of neutrals. However, the lines in Fig. 8 derived from the ion beam results show definite curvature and the averages value of the slopes, E_a', do not exactly correspond to the threshold energies in Eq. (12). For example, the slope of the pseudo-Arrhenius plot for reaction (1) at low energies yields $E_a' \approx 7$ meV, as compared to the threshold value of $E_T = 15.4$ meV. This deviation is *not* due to fundamental non-Arrhenius behavior, since it can be shown analytically that the true Arrhenius activation energy is identically equal to the threshold, i.e., $E_a = E_T$, for this particular form of the cross section, Eq. (12) with $n = 0.5$.[65] Rather, the nonthermal energy distributions are responsible for the deviation. The other model cross sections do exhibit curvature in a true Arrhenius plot and therefore have somewhat different curvature in the pseudo-Arrhenius plots (not shown). Furthermore, convolution over the ion energy spread (in addition to the thermal motion of the target gas) introduces additional curvature in the pseudo-Arrhenius plot and results in larger errors in the derived activation energy. Thus, the pseudo-Arrhenius analysis is not quantitatively valid for ion beam experiments. A critical assessment of its validity for conditions of flow/drift tube experiments would require detailed analysis of the ion energy distributions as a function of the drift field. The pseudo-Arrhenius presentation of the data can be useful for depicting qualitative differences of reactivity due to activation barriers, but can give only semiquantitative values of the true endothermicities.

DERIVATION OF ENDOTHERMICITIES

The endoergicity of reaction (1), combined with auxiliary thermochemical data, can be used to derive the bond energy $D_0^\circ(NH^+)$. Since this important bond energy is not accurately known spectroscopically, it is desirable to determine the endoergicity as accurately as possible from the ion–molecule reaction experiments. The threshold energies listed in Table II represent phenomenological endoergicities for the reactions. The spread of values obtained for different cross section models gives an indication of their experimental reliability. In the following, we discuss other possible sources of systematic errors in the results. Much of this discussion applies to the other recent determinations[17–19] of the reaction endoergicity as well as to the present work.

Rotational energy

As discussed above, the treatment of rotational energy is especially important in this system due to the small reaction endoergicity. The extent to which reactant rotational energy couples into the reaction coordinate will strongly influence the translational energy thresholds. This is demonstrated by the deviation between the threshold energies obtained by the empirical cross section models (which allow full coupling of reactant rotational energy) and those obtained from semiempirical classical PST (which constrains rotational promotion of the reaction according to angular momentum conservation). It would be desirable to determine the rotational dependence of the reactions experimentally. This may be possible in low-temperature or beam experiments by exploiting the different rotational populations of *ortho* and *para* hydrogen.

Electronic state of products

We have tacitly assumed that the $N^+ + H_2$ reaction produces ground state products. The $NH^+(^4\Sigma^-)$ electronic state of products lies only 0.06 eV above the $NH^+(^2\Pi)$ ground state.[66] Energetically, of course, only the ground state can be formed at the threshold. However, formation of the excited state could be a strongly competing process just above the threshold. This is particularly the case since the vibrational levels of the ground state are strongly perturbed by the upper state.[67] Moreover, the ground state of the NH_2^+ intermediate correlates[5] with the $NH^+(^4\Sigma^-) + H$ excited products in strict $C_{\infty v}$ (HNH^+) symmetry, although it adiabatically correlates with ground state products for other geometries via an avoided crossing. Competition between the two product channels could influence the shape of the cross sections at low energies and therefore affect the extraction of threshold energies. The PST calculations herein neglect the presence of excited product states.

Spin-orbit energy splittings

We have also neglected the spin-orbit splittings of $N^+(^3P_J)$ reactant and $NH^+(^2\Pi)$ product. The drift cell ion source presumably creates an approximately 300 K thermal population of the $^3P_0$ (0.0 meV), $^3P_1$ (6.1 meV), and $^3P_2$ (16.2 meV) spin-orbit states of N^+.[27] This gives an mean thermal energy of 9.5 meV. Assuming that spin-orbit energy is available to drive the reaction, the effective energy thresholds should be increased by this amount. Spin-orbit coupling could also affect the reactivity.[68] This seems unlikely, however, since the spin-orbit interactions are much smaller than the electrostatic interactions between approaching reactants in this case.

Similar considerations for the products may apply since $NH^+(^2\Pi)$ has both $J = 3/2$ and $J = 1/2$ spin-orbit components. The distribution of spin-orbit states in products is unknown. The spin-orbit coupling constant of $NH^+(^2\Pi)$ is 9.6 meV.[66]

Quadrupole moment of hydrogen

Molecular hydrogen has a permanent quadrupole moment and the charge–quadrupole potential ($V \propto r^{-3}$) is the leading term in the long-range potential. While the charge–induced dipole potential ($V \propto r^{-4}$) is always attractive, the charge–quadrupole potential is either attractive or repulsive depending on orientation. We have previously presented a frozen-rotor approximation to the collision cross section for the charge–quadrupole plus charge–induced dipole potential.[20] In near-perpendicular X^+–H_2 orientations, the collision cross section is larger than predicted by the LGS model for the charge–induced dipole potential alone. In near-collinear orientations, the cross section is smaller than LGS and even has a small energy threshold (a few meV). Therefore, if collinear orientations were strongly favored for some reason, the reaction might exhibit an apparent activation energy which does not correspond to an endothermicity. There are two arguments against such an effect in the present system. First, no strong orientational dependence is expected on the basis of the known features of the potential energy surfaces. Second, the variation of the experimental threshold energies due to zero-point energy differences would not be apparent if the thresholds were due to quadrupole repulsions. On the other hand, the anisotropic quadrupole term in the potential might affect the behavior of the cross section at low energies.[69,70] The PST calculations presented above neglect quadrupole terms in the calculation of the centrifugal barrier for the "loose" transition state between the complex and reactant or product channels.

Thermochemical values

It is difficult to quantify the influence of each of these effects. For a best estimate of the heats of reaction, ΔH°_0, we start with an average of the ΔE_e values given in Table II for three forms of the cross section model where rotational energy is explicitly considered, i.e., the two versions of Eq. (13) and PST. The mean ΔE_e, 106 ± 20 meV (± 2 standard deviations), is then readjusted for the known change in zero-point vibrational energy, $\Delta G(0)$, for each isotopic reaction. Finally, the values are adjusted by 9.5 meV to correct for the thermal spin-orbit energy of $N^+(^3P)$. This procedure gives the following values: $\Delta H^\circ_0 = 33 \pm 24$ meV for reaction (1), $\Delta H^\circ_0 = 61 \pm 30$ meV for reaction (2), $\Delta H^\circ_0 = 69 \pm 27$ meV for reaction (3a) and $\Delta H^\circ_0 = 19 \pm 27$ meV for reaction (3b). The error limits combine the uncertainty in the ΔE_e value and the (conservative) ± 0.1 eV lab uncertainty in the experimental energy scale. Despite the experimental difficulties in extraction of energy thresholds from the energy-broadened cross section data, the uncertainties are smaller in absolute terms than those usually quoted for threshold energies obtained by beam guide methods (typically ± 0.05 to ± 0.2 eV). This is because the low endoergicities and the isotopic variations restrict the threshold energies which can fit the data to a rather small range. However, the values depend somewhat on the cross section models used to analyze the experimental data. The error limits conservatively reflect this uncertainty. A better understanding of the threshold behavior in general and the rotational energy dependence in particular would allow a higher degree of precision.

The other recent determinations of the reaction endothermicities agree with the present values within the uncertainty limits. For reaction (1), the previous values are 22 meV from the gas jet experiment,[17] 18.5 meV for the ion trap experiment,[18] and 37 ± 3 meV from the SIFDT[19] experiments. These values are to be compared with $\Delta H^\circ_0 = 33 \pm 24$ meV from the present work. The previous values are all corrected to 0 K by adding in the mean rotational energy.[71] As discussed above, this correction assumes the rotational energy is entirely available to drive the reaction. This cannot be true and therefore the rotational correction is probably overestimated. The error limits placed on the value for ΔH°_0 from the present work include the uncertainty in the treatment of rotational energy.

Combining the well established heats of formation[26] $\Delta H^\circ_{f,0}(N^+) = 447.7$ kcal/mol and $\Delta H^\circ_{f,0}(H) = 51.63$ kcal/mol with the reaction enthalpy for reaction (1) obtained here, $\Delta H^\circ_0 = 33 \pm 24$ meV or 0.76 ± 0.55 kcal/mol, we can derive the heat of formation of NH^+, $\Delta H^\circ_{f,0}(NH^+)$

$= 396.8 \pm 0.6$ kcal/mol. This compares very favorably with a recent value obtained by Gibson, Green, and Berkowitz[30] from photoionization of NH_2, $\Delta H^\circ_{f,0}(NH^+) = 396.3 \pm 0.3$ kcal/mol. Using the values $\Delta H^\circ_{f,0}(N) = 112.534$ kcal/mol and $\Delta H^\circ_{f,0}(H^+) = 365.2$ kcal/mol,[26] we obtain the NH^+ bond energy $D^\circ_0(N\text{-}H^+) = 80.9 \pm 0.6$ kcal/mol (3.51 ± 0.03 eV). Finally, using the adiabatic ionization potential $IP(NH) = 13.49 \pm 0.01$ eV obtained by Dunlavey *et al.*[72] from photoelectron spectroscopy [Foner and Hudson[39] obtained $IP(NH) = 13.47 \pm 0.05$ eV from electron impact ionization threshold measurements], we can derive $\Delta H^\circ_{f,0}(NH) = 85.8 \pm 0.6$ kcal/mol and $D^\circ_0(NH) = 78.4 \pm 0.6$ kcal/mol (3.40 ± 0.03 eV).

CONCLUSION

Cross sections for the slightly endothermic reaction of $N^+(^3P)$ with H_2, HD, and D_2 to form NH^+ and ND^+ have been measured from thermal energies to 30 eV c.m. The results complement recent measurements of the reaction rates at 300 K[19] and at very low temperatures.[17,18]

The low energy behavior of the cross sections is characterized by deviations among the isotopic channels due to zero-point energy differences in the reaction endoergicities. This behavior has been analyzed using empirical cross section models and classical phase space theory to obtain threshold energies for each reaction. The threshold energy yields the reaction endothermicity, $\Delta H^\circ_0 = 0.033 \pm 0.024$ eV (0.76 ± 0.55 kcal/mol) for reaction (1), which agrees with recent independent determinations within its uncertainty. The largest source of uncertainty in the endothermicity is not the experimental uncertainty of the cross section data, but rather arises from uncertainties in modeling the threshold behavior and in making corrections for reactant internal energy. The reaction endothermicity is used to derive the heat of formation $\Delta H^\circ_{f,0}(NH^+) = 396.8 \pm 0.6$ kcal/mol, which is in good agreement with the value obtained in recent photoionization experiments by Gibson, Green, and Berkowitz.[30]

At high energies, the cross sections show behavior which is typical for ion–molecule reactions at energies where product dissociation becomes important. The energy dependence of the cross sections and isotope effects are consistent with the differential reactive scattering results of Mahan and co-workers.[1–5]

ACKNOWLEDGMENTS

We thank N. G. Adams, D. Smith, G. Dunn, and J. B. Marquette for helpful discussions. This research is supported by the National Science Foundation, Grant No. CHE-8608847.

[1]E. A. Gislason, B. H. Mahan, C.-W. Tsao, and A. S. Werner, J. Chem. Phys. **54**, 3897 (1971).
[2]J. A. Fair and B. H. Mahan, J. Chem. Phys. **62**, 515 (1975).
[3]J. M. Farrar, S. G. Hansen, and B. H. Mahan, J. Chem. Phys. **65**, 2908 (1976).
[4]B. H. Mahan and W. E. W. Ruska, J. Chem. Phys. **65**, 5044 (1976).
[5]S. G. Hansen, J. M. Farrer, and B. H. Mahan, J. Chem. Phys. **73**, 3750 (1980).
[6]G. Eisele, A. Henglein, P. Botschwina, and W. Meyer, Ber. Bungsenges. Phys. Chem. **78**, 1091 (1974).
[7]B. H. Mahan, Acc. Chem. Res. **9**, 55 (1975).
[8]S. Y. Chu, A. K. Q. Siu, and E. F. Hayes, J. Am. Chem. Soc. **94**, 2969 (1972).
[9]M. A. Gittins and D. M. Hirst, Chem. Phys. Lett. **35**, 534 (1975).
[10]M. A. Gittins and D. M. Hirst, Faraday Discuss. Chem. Soc. **62**, 67 (1977).
[11]D. M. Hirst, Mol. Phys. **35**, 1559 (1978).
[12]M. A. Gittins and D. M. Hirst, Chem. Phys. Lett. **65**, 507 (1979).
[13]C. F. Bender, J. H. Meadows, and H. F. Schaefer III, Faraday Discuss. Chem. Soc. **62**, 59 (1977).
[14]A. Dalgarno and J. H. Black, Rep. Prog. Phys. **39**, 573 (1976).
[15]N. G. Adams, D. Smith, and T. J. Miller, Mon. Not. R. Astron. Soc. **211**, 857 (1984).
[16]G. Gioumousis and D. P. Stevenson, J. Chem. Phys. **29**, 294 (1958).
[17]J. B. Marquette, B. R. Rowe, G. Duperyrat, and E. Roueff, Astron. Astrophys. **147**, 115 (1985).
[18]J. A. Luine and G. H. Dunn, Astrophys. J. **299**, L67 (1985).
[19]N. G. Adams and D. Smith, Chem. Phys. Lett. **117**, 67 (1985).
[20]K. M. Ervin and P. B. Armentrout, J. Chem. Phys. **83**, 166 (1985).
[21]K. M. Ervin and P. B. Armentrout, J. Chem. Phys. **84**, 6738 (1986).
[22]Kent M. Ervin, Ph.D. thesis, University of California, Berkeley, 1986.
[23]S. G. Hansen, Ph.D. thesis, University of California, Berkeley, 1980.
[24]P. A. M. VanKoppen, P. R. Kemper, A. J. Illies, and M. T. Bowers, Int. J. Mass Spectrom. Ion Proc. **54**, 263 (1983).
[25]Quenching of the excited states produced by 50 eV electron impact requires less than 3 ms at N_2 pressures of 10 mTorr. [W. Frobin, Ch. Schlier, K. Strein, and E. Teloy, J. Chem. Phys. **67**, 5505 (1977).]
[26]H. M. Rosenstock, K. Draxl, B. W. Steiner, and J. T. Herron, J. Phys. Chem. Ref. Data **6**, Suppl. 1 (1977).
[27]C. E. Moore, *Atomic Energy Levels*, Natl. Ref. Data Ser., Natl. Bur. Stand. No. 35 (U.S. GPO, Washington, D. C., 1935).
[28]I. Wendel, R. A. Friedel, and M. Orchin, J. Am. Chem. Soc. **71**, 1140 (1949).
[29]S. G. Lias, J. F. Liebman, and R. D. Levin, J. Phys. Chem. Ref. Data **13**, 695 (1984).
[30]S. T. Gibson, J. P. Greene, and J. Berkowitz, J. Chem. Phys. **83**, 4319 (1985).
[31]N. G. Adams, D. Smith, and J. F. Paulson, J. Chem. Phys. **72**, 288 (1980).
[32]The polarizability of hydrogen is $\alpha = 0.79 \times 10^{-24}$ cm^3 [J. O. Hirshfelder, C. R. Curtiss, and R. B. Bird, *Molecular Theory of Gases and Liquids* (Wiley, New York, 1954), p. 947].
[33]M. E. Weber, J. L. Elkind, and P. B. Armentrout, J. Chem. Phys. **84**, 1521 (1986).
[34]Fits to the experimental cross sections use $\sigma(E) = \sigma_0 \cdot E^{-m}$ as the cross section for formation of the diatomic product ion, which is then multiplied by the dissociation probability given by the decay model (Ref. 33) and convoluted over the experimental energy distributions. Other model parameters are $f = 1$ and $p = 1$ or $p = 2$, in the notation of Ref. 33.
[35]J. L. Elkind and P. B. Armentrout, J. Chem. Phys. **84**, 4862 (1986).
[36]A. Henglein and K. Lacmann, Adv. Mass Spectrom. **3**, 331 (1966); A. Henglein, in *Ion–Molecule Reactions in the Gas Phase*, edited by P. J. Ausloos (American Chemical Society, Washington, D. C., 1966), p. 63; A. Ding, K. Lacmann, and A. Henglein, Ber. Bunsenges. Phys. Chem. **71**, 596 (1967).
[37]D. R. Bates, C. J. Cook, and F. J. Smith, Proc. Phys. Soc. **83**, 49 (1964).
[38]T. F. Moran and B. P. Mathur, Phys. Rev. A **21**, 1051 (1980).
[39]S. N. Foner and R. L. Hudson, J. Chem. Phys. **74**, 5017 (1981).
[40]P. J. Chantry, J. Chem. Phys. **55**, 2746 (1971).
[41]C. Lifshitz, R. L. C. Wu, T. O. Tiernan, and D. T. Terwilliger, J. Chem. Phys. **68**, 247 (1978).
[42]J. D. Burley, K. M. Ervin, and P. B. Armentrout, J. Chem. Phys. (in press).
[43]P. B. Armentrout, in *Structure, Reactivity, and Thermochemistry of Ions*, NATO Adv. Study Institute Ser., edited by P. Ausloos, S. G. Lias, and D. Dixon (Reidel, Dordrecht, in press).
[44]R. D. Levine and R. B. Bernstein, J. Chem. Phys. **56**, 2281 (1972).
[45]R. D. Levine and R. B. Bernstein, *Molecular Reaction Dynamics* (Oxford, New York, 1974), p. 46.
[46]J. L. Elkind and P. B. Armentrout, J. Phys. Chem. **88**, 5454 (1984).
[47]G. Herzberg, *Molecular Spectra and Molecular Structure. I. Spectra of Diatomic Molecules* (Van Nostrand Reinhold, Princeton, 1950).
[48]Rotational populations are calculated for the 305 K reactant gas temperature, taking into account nuclear spin statistics.
[49]The correction using the mean rotational energy is certainly valid in cases

where the rotational energy is small relative to the translational energy threshold, for example, $C^+ + H_2 \rightarrow CH^+ + H$ (Ref. 21) and $Si^+ + H_2 \rightarrow SiH^+ + H$ (Ref. 46).

[50]W. H. Miller, J. Chem. Phys. **65**, 2216 (1976); K. Morokuma, B. C. Eu, and M. Karplus, *ibid.* **51**, 5193 (1969).

[51]J. C. Light and J. Lin, J. Chem. Phys. **43**, 3209 (1965); P. Pechukas, J. C. Light, and C. Rankin, *ibid.* **44**, 794 (1966); J. Lin and J. C. Light, *ibid.* **45**, 2545 (1966).

[52]E. Nikitin, Teor. Eksp. Khim. **1**, 135, 144, 428 (1965). [Theor. Exp. Chem. (Eng. Trans.) **1**, 83, 90, 275 (1975).]

[53]D. A. Webb and W. J. Chesnavich, J. Phys. Chem. **87**, 3791 (1984).

[54]W. J. Chesnavich and M. T. Bowers, J. Chem. Phys. **66**, 2306 (1977).

[55]K. M. Ervin and P. B. Armentrout, J. Chem. Phys. **84**, 6750 (1986).

[56]E. Herbst and S. K. Knudson, Chem. Phys. **55**, 293 (1981).

[57]In the notation of Refs. 55 and 56, the electronic degeneracy factors are $f = 3/9$ for the reactant channel and $f = 3/3$ for the product channel.

[58]J. L. Elkind and P. B. Armentrout, J. Phys. Chem. **89**, 5626 (1985).

[59]J. L. Elkind and P. B. Armentrout (unpublished).

[60]A. F. Wagner and D. G. Truhlar, J. Chem. Phys. **57**, 4063 (1972).

[61]Error limits are based on the 25% uncertainty cited for SIFDT experiments [D. Smith, N. G. Adams, and E. Alge, Chem. Phys. Lett. **105**, 317 (1984)].

[62]D. Smith (private communication); G. Dunn (private communication).

[63]Rates for 10 K are interpolated from the low temperature results for comparison with the PST rates.

[64]D. L. Albritton, I. Dotan, W. Lindinger, M. McFarland, J. Tellinghuisen, and F. C. Fehsenfeld, J. Chem. Phys. **66**, 410 (1977); L. A. Viehland and E. A. Mason, *ibid.* **66**, 422 (1977); S. L. Lin and J. N. Bardsley, *ibid.* **66**, 435 (1977).

[65]M. Menzinger and R. Wolfgang, Angew. Chem. Int. Ed. **8**, 438 (1969).

[66]K. P. Huber and G. Herzberg, *Constants of Diatomic Molecules* (Van Nostrand Reinhold, New York, 1979).

[67]L. Farnell and J. F. Ogilivie, J. Mol. Spectrosc. **101**, 104 (1983).

[68]For a discussion of spin-orbit effects on the reactivity of ion–molecule reactions, see K. M. Ervin and P. B. Armentrout, J. Chem. Phys. **85**, 6380 (1986).

[69]The analysis of the ion trap experiment (Ref. 18) relies on the LGS model as an estimate of the collision rate to derive the reaction rate from the measured reaction probability. Since the quadrupole term may change the overall collision rate, especially for low diatomic rotational states, this treatment could be inaccurate. Approximate collision models which include the quadrupole terms in the long-range potential have been discussed [T. Su and M. T. Bowers, Int. J. Mass Spectrom. Ion Phys. **17**, 309, 424 (1976); Ref. 20].

[70]In contrast to the present case, the $C^+ + H_2 \rightarrow CH^+ + H$ reaction (Refs. 21 and 55) has a 0.4 eV translational energy threshold; at that energy the quadrupole interaction is probably not critically important.

[71]No further corrections are made for the $N^+(^3P)$ spin-orbit energy. Only ground state $N^+(^3P_0)$ is present in the low-temperature experiments (Refs. 17 and 18), but a thermal spin-orbit state population is present in the SIFDT experiments. Correcting for spin-orbit energy in the SIFDT value gives $\Delta H^\circ_0 = 46$ meV.

[72]S. J. Dunlavey, J. M. Dyke, N. Jonathan, and A. Morris, Mol. Phys. **39**, 1121 (1980).